# PARASHIFT Probes: Solution NMR and X-ray Structural Studies of Macrocyclic Ytterbium and Yttrium Complexes

Kevin Mason[a], Nicola J. Rogers[a] , Elizaveta A. Suturina[b], Ilya Kuprov[b], Juan A. Aguilar[a], Andrei S. Batsanov[a], Dmitry S. Yufit[a] and David Parker[a]*

a) Department of Chemistry, Durham University, South Road, Durham UK, DH1 3LE.

b) School of Chemistry, University of Southampton, Highfield, Southampton UK SO17 1BJ.

## ABSTRACT

Ytterbium and yttrium complexes of octadentate ligands based on 1,4,7,10-tetraazacyclododecane with a coordinated pyridyl group and either tricarboxylate ($L^1$) or triphosphinate ($L^2$) donors form twisted square antiprismatic structures. The former crystallises in the centrosymmetric group, $P2_1/c$, with the two molecules related by an inversion centre, whereas the latter was found as an unusual kryptoracemate in the chiral space group, $P2_1$. Pure shift NMR and EXSY spectroscopy allowed the dynamic exchange between the (*RRR*)-*Δ*-(*δδδδ*) and (*RRR*)-*Λ*-(*λλλλ*) TSAP diastereomers of the [Y.$L^2$] complex to be detected. The rate limiting step in the exchange between *Δ* and *Λ* isomers involves cooperative ligand arm rotation. Detailed analysis of NOESY, COSY, HSQC and HMBC spectra confirms that the major conformer in solution is (*RRR*)-*Λ*-(*λλλλ*), consistent with crystal structure analysis and DFT calculations. The magnetic susceptibility tensors for [Yb.$L^1$] and [Yb.$L^2$], obtained from pseudocontact shift analysis, are very different in agreement with a CASSCF calculation. The very different pseudocontact shift behaviour is explained by the change in the orientation of the pseudocontact shift field, as defined by the *β* angle of the susceptibility tensor.

## INTRODUCTION

Polyaza macrocyclic ligands with eight or nine donor atoms are known to form kinetically stable complexes with rare earth elements. [1,2] Over the past 30 years, they have found use in analytical, biochemical and clinical applications, ranging from the widespread adoption of gadolinium contrast agents in magnetic resonance imaging, [3] to their role in radioimmunotherapy and radioscintigraphy using complexes or conjugates labelled with $^{90}$Y, $^{153}$Sm, $^{149}$Tb or $^{177}$Lu. [4] In each of these cases, premature release of the metal ion must be avoided at all costs – both the free ligands and the lanthanide ions are toxic.

In recent work examining the scope and utility of paramagnetic metal complexes in magnetic resonance shift imaging, examples of temperature probes based on complexes of Fe(II), Co(II) or lanthanide(III) ions have been described. [5, 6-12] A key property of these complexes is that the chemical shift of a reporter nucleus in the ligand gives information not only about its position relative to the paramagnetic ion, but also about local temperature. [5-12] By careful ligand design, the chemical shift of a given reporter nucleus can also be made to report local pH simultaneously, [13-15] or indeed pM or pX, in the general cases, [16] provided that care is taken to design the coordinating ligand rationally.

A key design objective is to create a metal complex that exists as one preferred stereoisomer that is conformationally rigid on the NMR timescale, so that exchange broadening is minimised. Strategies that lead to preferential formation of one solution isomer, or slow down intramolecular motion, have been considered before. [17] For example, the series of octadentate ligands based on mono-substituted triphosphinate derivatives of 1,4,7,10-tetra-azacyclododecane (*i.e.* cyclen or 12-$N_4$) have been studied in detail. [18-20] Preferred formation of one relatively rigid isomer (out of 32 possible isomers) was established back in 1995, [18] and the reasons for this selectivity can be traced to the need to minimise the steric hindrance around the metal centre, in which the relative position of the three phosphinate substituents (*e.g.* Me, Bn or Ph) and the large bite angle associated with the three N-C-P-O-Ln 5-membered chelate rings are of paramount importance. No directly relevant crystal structures have been reported of monomeric lanthanide(III) triphosphinate complexes, based on octadenate ligands.

**Chart 1** Structures of the yttrium and ytterbium complexes examined in this study

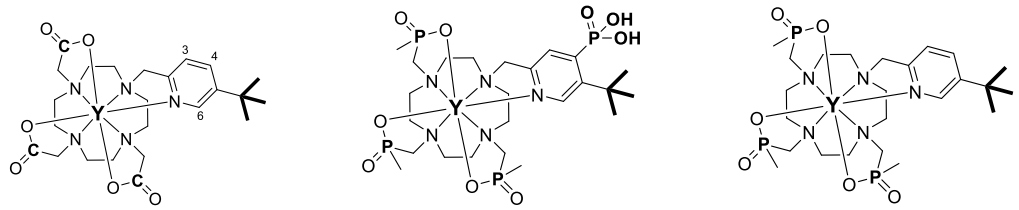

**[Y.L$^1$]** **[Y.L$^2$]** **[$H_2$Y.L$^3$]**

Very recently, the later lanthanide (Tb, Dy, Ho, Er, Tm) complexes have been created of such ligands, substituted with a “reporter” *t*-butyl group located just over 6 Å away

from the metal ion (Chart 1). Their scope as PARASHIFT probes is being evaluated [21,22], driven by the prospect of using them, or their simple conjugates with a targeting vector, for the assessment of local temperature and pH in dual or triple proton MRI imaging studies.

The complexes exhibit $^{1}$H NMR paramagnetic shifts of the *t*-butyl resonance in [Ln.L$^{2}$] that are 3 to 4 times larger than in the [Ln.L$^{1}$] complexes. Thus, the reporter *t*-butyl signal in [Ln.L$^{2}$] resonates over the range +76 ppm (Tm) to –83 ppm (Dy/Tb) at 295 K, with rates of relaxation of the $^{t}$Bu reporter group varying from 80 to 200 s$^{-1}$ at 7 Tesla, permitting the use of fast pulse repetition rates in imaging and chemical shift imaging experiments. A 15 to 25-fold signal intensity gain over the diamagnetic controls can then be obtained in imaging experiments. The paramagnetic probes can be administered at doses of the order of 0.1 mmole/kg, giving sufficient signal to allow the fate of the complex *in vivo* to be tracked, or to obtain regional temperature or pH maps. These doses are similar to those of the ubiquitous Gd complexes that are safely used in millions of MRI scans every year.

Here, we present X-ray structures for [Yb.L$^{1}$] and [Yb.L$^{2}$], and examine their diamagnetic Y(III) analogues to establish their solution-state structures and conformational exchange dynamics. We examine the origins of the differing shift behaviour of [Yb.L$^{1}$] and [Yb.L$^{2}$] as models for the remaining series, by studying the pseudocontact shift field in detail, relating behaviour to the nature of the magnetic susceptibility tensor. We also report the properties of Yb and Y complexes of the 4-phosphonate derivative of L$^{2}$ – those are important examples of complexes exhibiting temperature- and pH-dependent chemical shifts, for which parallel administration of the Tm and Dy analogues has recently allowed triple imaging studies *in vivo*, simultaneously reporting pH and temperature, as well as detailing anatomy *via* co-observation of the water signal. [22]

## RESULTS AND DISCUSSION

The ligands L$^{1-3}$ and their complexes were prepared using previously reported methods. [19, 22] Crystals of the Yb complexes were grown by diffusion of diethyl ether into a methanol solution for [Yb.L$^{1}$], and into an ethanol solution for [Yb.L$^{2}$], (Figures 1 and 2, and ESI: Figures S16, S19, S20). Crystal structures show a common twisted

square anti-prismatic coordination geometry with the Yb ion bound to the four ring nitrogen atoms, the pyridine nitrogen atom and the three anionic oxygen atoms.

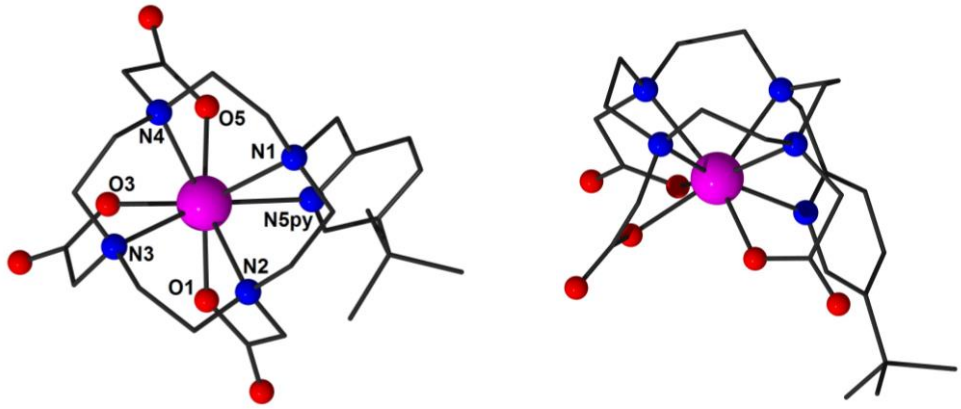


**Figure 1** Molecular structure of *Δ*–(*δδδδ*)-[Yb.L$^1$], viewed down the 12-N$_4$ ring (*left*) and from the side (*right*). H atoms omitted for clarity; the enantiomer was also present in the unit cell, CCDC-1502162.

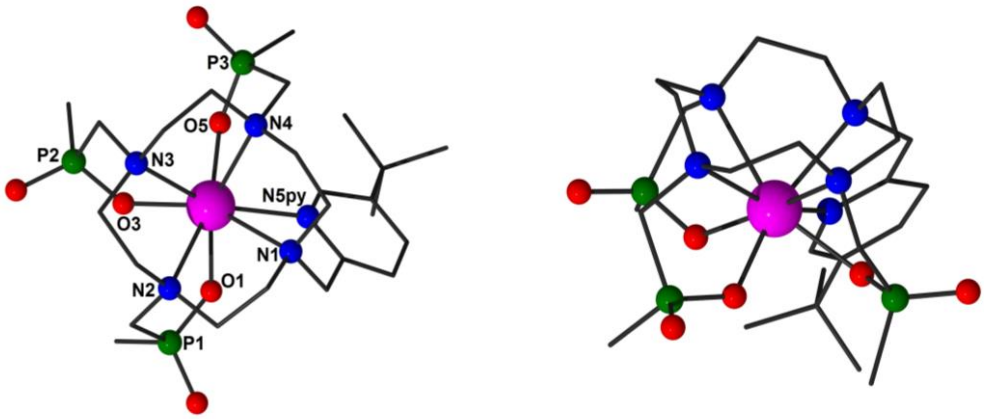


**Figure 2** Molecular structure of (*RRR*)-*Λ*–(*λλλλ*) [Yb.L$^2$], viewed down the 12-N$_4$ ring (*left*) and from the side (*right*). Hydrogen atoms and disorder in the *tert*-butyl pyridine group are omitted for clarity. The complex (*SSS*)-*Δ*–(*δδδδ*) [Yb.L$^2$] was also present in the unit cell. The bond distances in the two enantiomeric molecules are, respectively: Yb1-P1, 3.3312(16) & 3.3410(15); Yb1-P2, 3.3856(15) & 3.3714(14); Yb1-P3, 3.3548(16) & 3.3710(16) Å, in agreement with values calculated in related structures, by examining the field dependence of their $^{31}$P NMR relaxation rates, [18] CCDC-1501473.

Bond distances were systematically shorter between Yb and oxygen in the triphosphinate compared to the tricarboxylate complex, and were correspondingly longer to each of the nitrogen donor atoms. Such behaviour reflects both the preference for the anionic phosphinate oxygen donor and the need for the Yb ion to sit higher above the

12-ring $N_4$ plane, in order to allow cooperative ligation of the four nitrogen substituents. [23]

**Table 1.** Bond distances in the $N_5O_3$ coordination sphere for [Yb.L$^1$] and [Yb.L$^2$]

| Bond | Bond distance (Å) | |
|---|---|---|
| | [Yb.L$^1$] | [Yb.L$^2$]$^a$ |
| Yb1-O1 | 2.242(3) | 2.212(4) |
| Yb1-O3 | 2.249(3) | 2.221(4) |
| Yb1-O5 | 2.243(3) | 2.206(4) |
| Yb1-N1 | 2.521(3) | 2.557(6) |
| Yb1-N2 | 2.515(3) | 2.592(6) |
| Yb1-N3 | 2.507(3) | 2.613(4) |
| Yb1-N4 | 2.515(3) | 2.638(5) |
| Yb1-N5py | 2.485(3) | 2.569(3) |

a) average for the two molecules in the unit cell.

The torsion angles in the four NCCN chelate rings associated with the 12-$N_4$ ligand are of the same sign in each case, defining the $\lambda/\delta$ configurations reported in Tables 2 and 3. Similarly, $NCCN_{py}$ and NCCO torsion angles define the $\Delta/\Lambda$ configuration ($\Delta$ is equivalent to *P* helicity). The smaller twist angle of the "twisted" square-antiprism, (Table 3, averaging ~26°) compared to the "regular" square antiprism (typically ~40°) has been observed many times before, notably in the four-fold symmetric $N_4O_4$ complexes of the analogous carboxylate and phosphinate ligands, that lack a coordinating pyridine group. [24]

The complex [Yb.L$^1$] crystallised in a centrosymmetric space group ($P2_1/c$), so that both enantiomers were present and symmetry related. Examples of tricarboxylate and triphosphinate derivatives of 12-$N_4$ have been reported previously, but are restricted to dimeric species based on heptadentate ligands for triphosphinate derivatives. Tricarboxylate examples are more prevalent and varied, but only three octadentate ligands crystallise as 8-coordinate tricarboxylate species. [25,26] [Yb.L$^2$] is an interesting case of a kryptoracemate, [27] crystallizing in a chiral (Sohncke) space group $P2_1$, but with both enantiomers present as symmetrically positioned independent molecules.

The structure also resembles space group $P2_1/c$, in which it can be crudely refined, by assuming extensive disorder. [28,29]

**Table 2.** Torsion angles in the 12-$N_4$ ring (N-C-C-N) for [Yb.L$^1$] and [Yb.L$^2$].

| Torsion chain | Torsion angle (°) | | |
|---|---|---|---|
| | **[Yb.L$^1$]** [a] | **[Yb.L$^2$]** ($\lambda\lambda\lambda\lambda$) | **[Yb.L$^2$]** ($\delta\delta\delta\delta$) |
| N1-C1-C2-N2 | ±56.7(5) | –58.4(8) | 62.9(7) |
| N2-C3-C4-N3 | ±55.7(5) | –58.3(7) | 59.2(7) |
| N3-C5-C6-N4 | ±56.9(5) | –55.3(8) | 57.5(7) |
| N4-C7-C8-N1 | ±58.3(5) | –59.2(7) | 57.7(7) |

[a] + and –, respectively, for $\delta\delta\delta\delta$ and $\lambda\lambda\lambda\lambda$ enantiomers, inversion-related in space group $P2_1/c$

**Table 3.** Torsion angles around the exocyclic groups for [Yb.L$^1$] and [Yb.L$^2$].

| Torsion chain | Torsion angle (°) | | |
|---|---|---|---|
| | **[Yb.L$^1$]** [a] | **[Yb.L$^2$]** ($\Lambda$) | **[Yb.L$^2$]** ($\Delta$) |
| N1-C15-C16-N5py | 25.9(6) | –28.5(9) | 30.0(9) |
| N2-C9-C10(P1)-O1 | 21.8(6) | –29.2(5) | 27.3(6) |
| N3-C11-C12(P2)-O3 | 21.6(5) | –31.2(4) | 33.7(4) |
| N4-C13-C14(P3)-O5 | 21.0(6) | –48.0(4) | 46.8(4) |

[a] + and –, respectively, for $\Delta$ and $\Lambda$ enantiomers, inversion-related in space group $P2_1/c$

**Table 4.** Twist angles between the $NO_3$ and $N_4$ coordination faces of [Yb.L$^1$] and [Yb.L$^2$].

| Plane | Angle (°) | |
|---|---|---|
| | **[Yb.L$^1$]** | **[Yb.L$^2$]**[a] |
| N1-Yb-N3 *vs* N5py-Yb-O3 | 25.1 | 25.7 |
| N5py-Yb-O3 *vs* N4-Yb-N2 | 65.0 | 65.4 |
| N4-Yb-N2 *vs* O5-Yb-O1 | 26.6 | 27.0 |
| O5-Yb-O1 *vs* N1-Yb-N3 | 63.6 | 64.6 |

a) average for the two independent molecules

**DFT Studies**

The relative free energies of the possible isomeric yttrium complexes of [Y.L$^2$] were computed using DFT methods. In gas phase geometry optimisations, the two lowest energy structures found (Table 5) were the square anti-prismatic (*RRR*)-*Λ*–(*δδδδ*) and the twisted square anti-prismatic (*RRR*)-*Λ*–(*λλλλ*) isomers. The other two diastereomers with an (*RRR*)-*Δ* configuration were about 20 kcal/mol higher in energy, reflecting the destabilisation of the overall structure as a result of unfavourable steric interactions involving the P-methyl groups, pointing towards the 12-$N_4$ ligand, with the more exposed phosphorus oxygen groups.

**Table 5.** Calculated relative enthalpies and free energies for diastereoisomers of [Y.L$^2$]

| | BP86 (gas phase) | | M06-2X (gas phase) | | M06-2X (water SMD) | |
|---|---|---|---|---|---|---|
| Complex isomer | $\Delta H_0$ kcal/mol | $\Delta G_{298}$ kcal/mol | $\Delta H_0$ kcal/mol | $\Delta G_{298}$ kcal/mol | $\Delta H_0$ kcal/mol | $\Delta G_{298}$ kcal/mol |
| (*RRR*)-*Λ*-(*δδδδ*) SAP | 0 | 0 | 2 | 3 | 5 | 7 |
| (*RRR*)- *Λ*-(*λλλλ*) TSAP | 0 | 1 | 0 | 0 | 0 | 0 |
| (*RRR*)-*Δ*-(*δδδδ*) TSAP | 18 | 18 | 17 | 17 | 3 | 3 |
| (*RRR*)- *Δ*-(*λλλλ*) SAP | 23 | 23 | 24 | 25 | 12 | 11 |

However, the presence of a polarisable continuum solvent (M06-2X with SMD water) stabilises the pair of (*RRR*)-*Δ* isomers: the phosphinate oxygen atoms gain more negative charge (Mulliken point charges increase from –0.5 to –0.65) and the average Ln-O bond length increases from ~2.2 to ~2.3 Å, causing the methyl groups to be further away from the 12-$N_4$ ligand. In the (*RRR*)-*Λ* pair of diastereomers, solvation stabilisation is less pronounced, with the phosphinate groups partially shielded by the macrocyclic 12-$N_4$ ligand.

DFT Calculations in a polarisable continuum solvent were also run for [Y.L$^1$], comparing the stability of the SAP *Δ*–(*λλλλ*) and the TSAP *Λ*–(*λλλλ*) diastereomers, both in the absence (CN = 8) and presence (CN =9) of an axial coordinated water molecule. The SAP isomer preferred to be 9-coordinate, with a water-Y(III) distance of 2.56 Å. With the TSAP isomer, the complex was also formally 9-coordinate, but the nearest water ended up being hydrogen bonded to the coordinated carboxylate ox-

ygen, and the distance of 3.23 Å from the Y(III) ion is consistent with the idea of "partial hydration" [18b] in which there is a rather long Y(III)-water distance, that corresponds to a *q* value of the order of 0.25. This study therefore reaffirms the early hypothesis concerning partial hydration numbers, in which both short Ln-O bonds and classical $q$ = 1 behaviour, and long Ln-O bonds, *i.e.* partial (non-classical) hydration states may occur, determined by the nature of the local coordination environment. [18b, 18c] In each case, the overall free energy of binding associated with hydration is relatively small, ~2 kcal/mol. The lowest energy form was calculated to be the TSAP form (as also observed by crystallography) but the nine-coordinate SAP structure was only 1.5 kcal/mol higher in energy.

The DFT studies have thus suggested that the favoured solution isomers for [Y.L$^2$] and [Y.L$^1$] are the 8-coordinate (*RRR*)-$\Lambda$–($\lambda\lambda\lambda\lambda$) twisted square anti-prismatic (TSAP) structures, that are also observed in the crystal structures. For [Y.L$^2$], the (*RRR*)-$\Delta$–($\delta\delta\delta\delta$) TSAP diastereomer is of comparable energy. The error in these calculations is of the order of a few kcal/mol, [30] and so several isomeric complexes may be expected to be observed in solution by NMR spectroscopic methods.

**Solution NMR of yttrium(III) complexes: static and dynamic analysis**

$^1$H and $^{31}$P NMR spectra were analysed for the diamagnetic yttrium(III) complexes prior to the examination of the ytterbium(III) complexes, whose structure had been determined by X-ray crystallography.

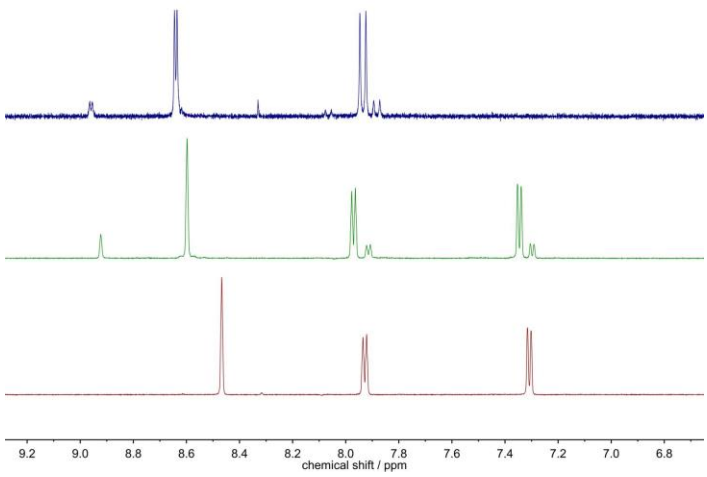

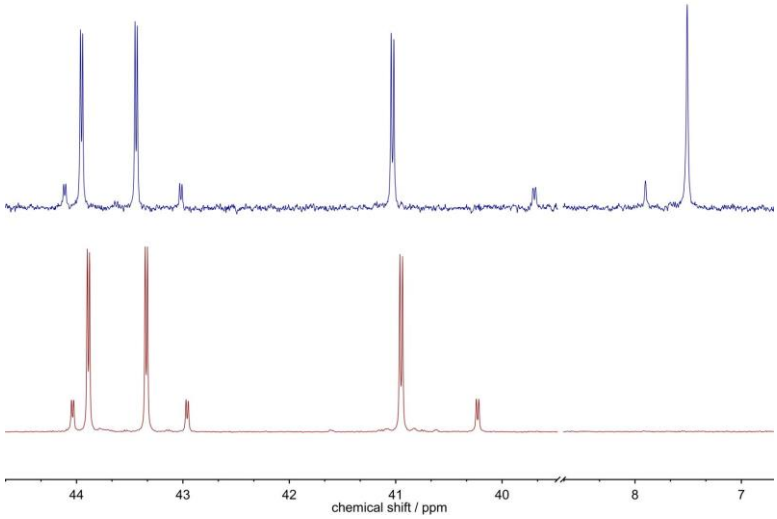


**Figure 3.** (*upper*) $^{1}$H NMR spectra (600 MHz, $D_2O$, pD 7.4, 295 K), of the pyridyl ring protons of [Y.L$^{1}$] (*red*), [Y.L$^{2}$] (*green*), and [Y.L$^{3}$] (*blue*), revealing two major isomers for each phosphinate complex; (*lower*) $^{31}$P{$^{1}$H} NMR spectra (14.1 T, $D_2O$, 298 K), of [Y.L$^{2}$] (*red*), and [Y.L$^{3}$] (*blue*), showing the major and minor isomers and the small $^{89}$Y-$^{31}$P couplings.

$^{1}$H NMR analysis of [Y.L$^{2}$] and [$^{2}$HY.L$^{3}$]$^{-}$ in $D_2O$ solution revealed that there are two sets of resonances for each pyridine ring proton in the triphosphinate complexes, in a ratio of 1:5 and 1:7, respectively (Figure 3). In contrast, analysis of the $^{1}$H NMR spectrum of the tricarboxylate complex, [Y.L$^{1}$], was consistent with the presence of one major species in solution. Alternatively, two or more species may be present in soluteon, in relatively fast exchange on the NMR timescale (see also ESI: Figures S8, S10, S11 and *vide infra*). Indeed the NOESY spectrum for [Y.L$^{1}$] at 295K showed that the diastereotopic pyridyl $NCH_2$ resonances at 4.26 and 3.84 ppm were undergoing chemical exchange, as the sign of the $^{1}$H-$^{1}$H cross peaks was the same as the sign of the diagonal, consistent with a pair of resonances undergoing chemical exchange. In contrast the $^{1}$H-$^{1}$H cross peak was of opposite sign for the pyridyl hydrogens, $H_3$ and $H_4$, resonating at 7.93 and 7.31 ppm (ESI, Figure S11), consistent with a classical nuclear Overhauser through-space effect.

It has been established that cooperative 12-$N_4$ ring inversion occurs at a rate of about 50 to 200 s$^{-1}$ (298 K), and leads to formal exchange between 'axial' and 'equatorial' ring hydrogens and adjacent ring carbons in the $\lambda\lambda\lambda\lambda$ and $\delta\delta\delta\delta$ isomers. [17,18] In contrast, cooperative arm rotation of the exocyclic N substituents interchanges $\Delta$ and $\Lambda$

isomers and usually occurs much more slowly, and exchanges the exocyclic methylene hydrogens, *i.e.* the $CH_2CO$ or $CH_2PO$ hydrogen atoms in this case. [23,24]

The three phosphinate atoms in [Y.L$^2$] and [HY.L$^3$]$^-$ are chemically non-equivalent, and a major and minor isomer was also observed, in each case, by $^{31}$P NMR spectroscopy. These isomers were in slow exchange on the NMR timescale (Figure 3 and SI Figure S9). Through-bond *J* coupling was observed from $^{89}$Y ($I$ = 1/2, 100% abundance) to each phosphinate $^{31}$P nucleus, ($^2J_{YP}$ = 5 Hz), giving rise to a series of doublets in the range 45 to 39 ppm, whereas the phosphonate $^{31}$P resonance in [Y.L$^3$] is too far away (5 bonds) from Y for any coupling to be observed (singlets at 7.5 ppm and 7.9 ppm for the major and minor isomer respectively). The presence of the phosphonate group at the 4-position of the pyridine ring in [HY.L$^3$]$^-$ has little effect on the $^{31}$P chemical shifts of the phosphinate groups, except for the minor isomer peak at 39.7 ppm (shifted from 40.2 ppm in [Y.L$^2$]). Taken together, these data, along with the pH dependence of the 41.0/39.7 ppm pair of $^{31}$P resonances, suggest that the major $^{31}$P peak at ~41 ppm is the one that is closest to the pyridine ring (ESI: Figures S6 and S7).

Detailed proton NMR assignments for each yttrium complex were made with the aid of $^1$H-$^{13}$C HSQC, $^1$H-$^{31}$P HMBC, $^1$H-$^{13}$C HMBC as well as pure shift NMR experiments (ESI; Figures S1–5, S8). The resonances associated with each of the three phosphinate arms for the triphosphinate complexes, [Y.L$^2$] and [HY.L$^3$]$^-$, were assigned (SI Table S2, and Experimental section). The pH dependence of the single $PCH_2N$ arm in [HY.L$^3$]$^-$ is associated with protonation of the phosphonate group on the pyridine moiety, for which the p$K_a$ has been established to be 7.15(6) (295K, I = 0) [22] in the Dy, Ho, Er and Tm(III) complexes. These ions are of near-identical ionic radius to Y(III).

Full assignment of all 31 chemically distinct protons of [Y.L$^2$] (Table S2) was undertaken by detailed analysis of all available NMR data. Pure shift $^1$H NMR techniques [31] proved to be very useful, and in the present case the removal of the $^1$H-$^1$H splitting was achieved using the PSYCHE pulse sequence; [34] $^1$H-$^{31}$P splitting was removed by standard $^{31}$P decoupling methods (Figure 4).

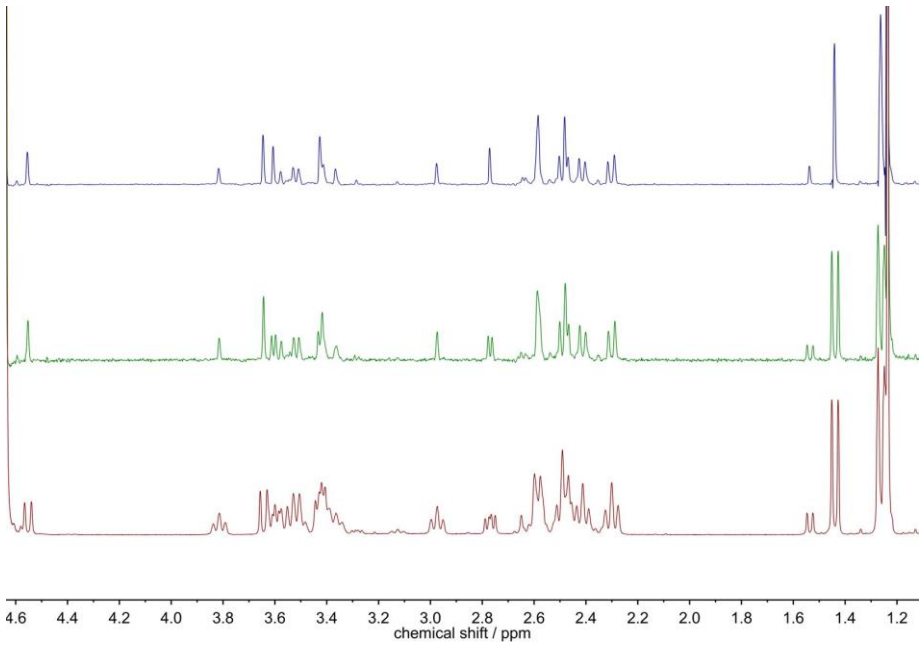


**Figure 1.** $^{1}$H (*red*), $^{1}$H {1H decoupled} (*green*), and $^{1}$H{1H and $^{31}$P decoupled} (*blue*) NMR spectra (14.1 T, $D_2O$, pD 6, 295 K), for the triphosphinate complex, [Y.L$^{2}$], in the shift range 1.1 to 4.6 ppm.

There is only one [Yb.L$^{2}$] conformer namely (*RRR*)-*Λ*-(*λλλλ*) that does not contradict the observed NOESY spectrum (Figure 2). Each methyl group has only two NOE cross-peaks with axial and equatorial protons of corresponding arms. The absence of additional cross-peaks with cyclen protons rules out (*RRR*)-*Δ*-(*δδδδ*) and (*RRR*)-*Δ*-(*λλλλ*) conformers because in these cases, the methyl groups are closer to cyclen than to the exocyclic $CH_2$ protons (ESI Figure S7 ). The other important feature in the NOESY spectrum is the presence of two cross-peaks for the axial proton of the pyridine arm at 4.55 ppm with cyclen protons attached to different carbons; such a feature rules out the presence of the (*RRR*)-*Λ*-(*δδδδ*) conformer, because it has only neighbouring cyclen protons that are attached to the same carbon (ESI Figure S8).

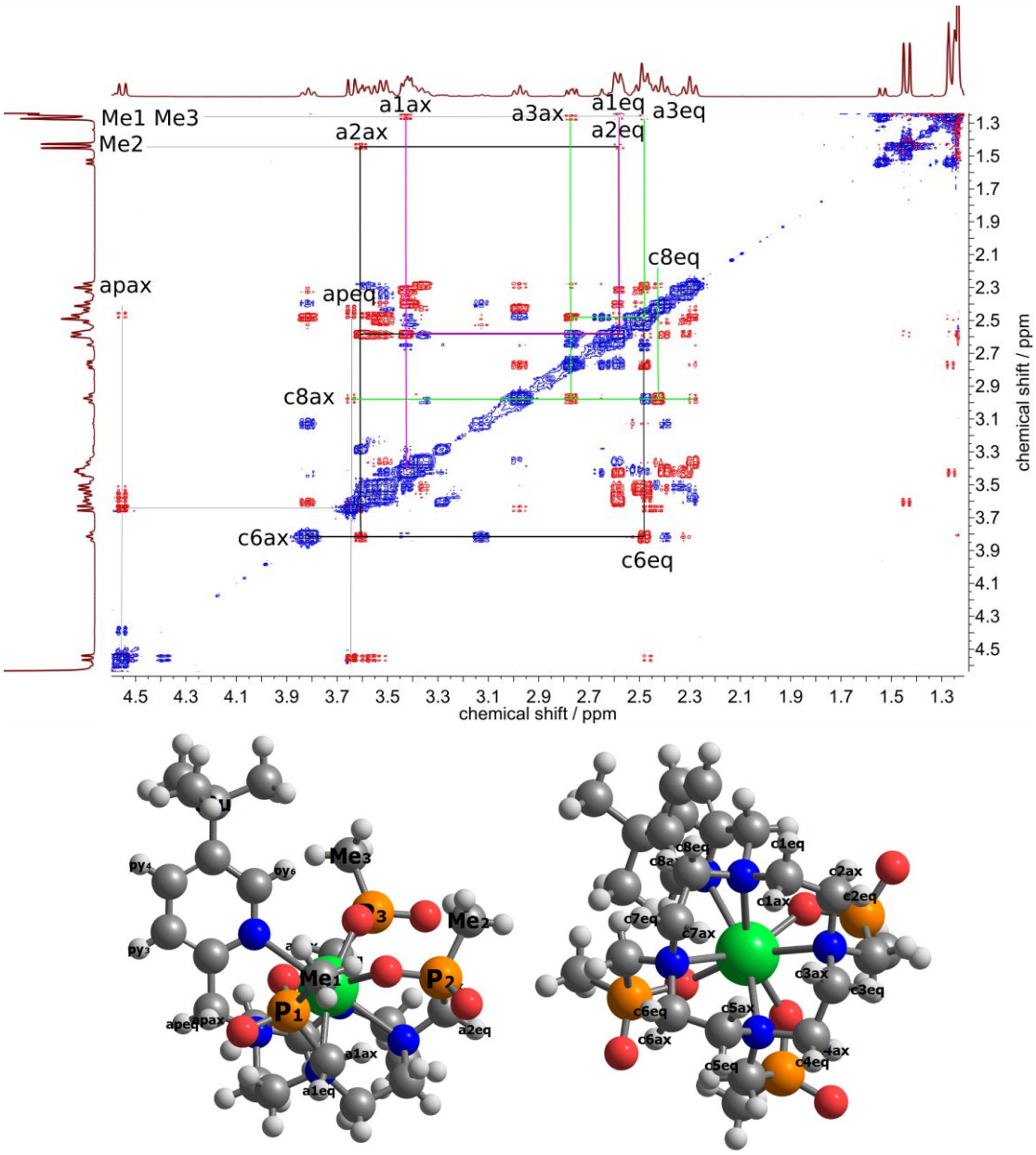


**Figure 2.** (*upper*): $^{1}$H-$^{1}$H 2D NOESY/EXSY NMR spectrum (14.1 T, $D_2O$, 298 K, mixing time = 300 ms), of the aromatic protons of [Y.L$^{2}$], showing exchange correlations (blue) as well as through-space correlations (red). Important NOE cross-peaks that suggest (*RRR*)-Λ-(*λλλ*) conformation are highlighted (see text for the discussion); (*lower*) Labels for atoms used in the assignment tables. The cyclen protons and carbons are labeled with 'c' and ordered clockwise, where 'ax' stands for axial and 'eq' stands for equatorial protons. Exocyclic methylene protons are labeled with 'a' and numbered the same way; pyridine arm is labeled 'ap'.

Through-space NOE correlations were observed between $H_4$ and $H_3$, out-of-phase with the diagonal, due to the close proximity of these two protons. Evidence for exchange was observed between the singlets at 8.92 ($H_6$, minor) and 8.60 ($H_6$, major), doublets at 7.97 ($H_4$ major) and 7.91 ($H_4$ minor), and doublets at 7.35 ($H_3$ major) and

7.30 ($H_3$ minor), (Figure 5), showing that these are the same pyridine protons in the two different conformational isomers of [Y.L$^2$]. Similar observations were seen in [HY.L$^3$]$^-$ : $H_6$ = 8.64 ppm (major) and 8.96 ppm (minor); $H_3$ = 7.93 ppm (major), and 7.88 ppm (minor). Additionally, $^{31}$P exchange was observed for [$^2$HY.L$^3$]$^-$, (ESI: Figure S12).

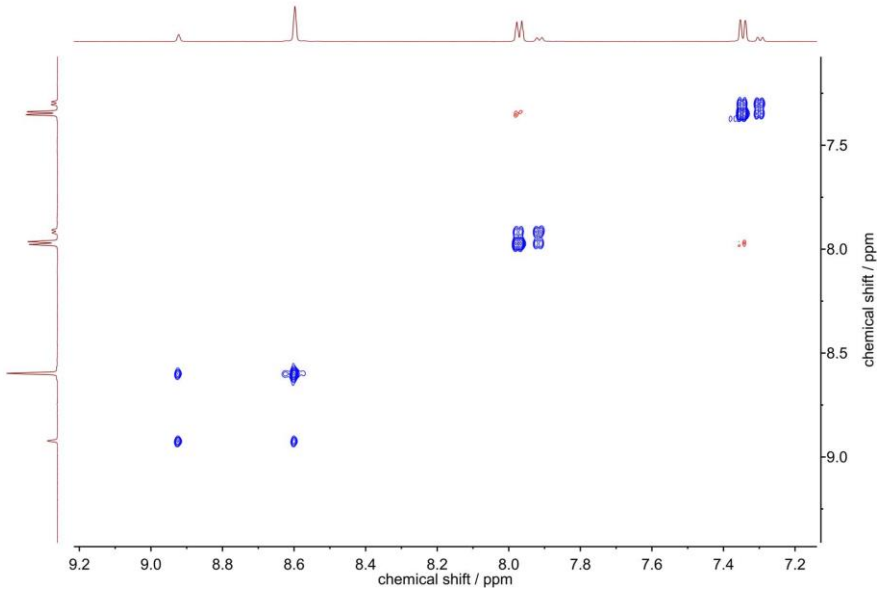


**Figure 3**. $^1$H-$^1$H 2D NOESY/EXSY NMR spectrum (14.1 T, $D_2O$, 298 K, mixing time = 300 ms), of the aromatic protons of [Y.L$^2$], showing exchange correlations (*blue*) as well as through-space correlations (*red*).

Exchange spectroscopy (EXSY) calculations were performed using the MestreNova EXSYCalc programme, using the data obtained from two EXSY spectra, one with a mixing time of zero ms and another with a mixing time of 300 ms. The rate of exchange between the minor and the major isomer was of the order of 1.1 to 1.4 s$^{-1}$. The reverse rates were slower, and fell in the range 0.17 to 0.23 s$^{-1}$, (Table 5).

**Table 5** EXSY exchange rates between isomers for [Y.L$^2$] and [HY.L$^3$]$^-$ (295K, $D_2O$, pD 7)

| **Complex** | **Exchange pair** | $k$ / s$^{-1}$ | $k^{-1}$ / s$^{-1}$ | $K_{eq}$ |
|---|---|---|---|---|
| [Y.L$^2$] | H$^6$ (pyridine $^1$H) | 1.13(3) | 0.23(2) | 4.9(3) |
| [Y.L$^3$] | H$^6$ (pyridine $^1$H) | 1.38(3) | 0.18(2) | 7.7(5) |
| [Y.L$^3$] | $^{31}$P phosphinate (41.0-39.7 ppm pair) | 1.34(4) | 0.16(2) | 8.4(5) |

Functionalisation at the 4'-position of the pyridine ring does not significantly alter the rate at which the two conformational isomers interconvert. The equilibrium constant for [Y.L$^2$] is 4.9(3), whereas that of [HY.L$^3$]$^-$ is larger, averaging 8.0(5), in reasonable agreement with the different isomer ratios observed (5:1 and 7:1) for the major and minor species by integration of the fully relaxed NMR spectra of each complex.

**Pseudocontact shift analysis** Two conformers are observed for each complex with a ratio of 3:1 for [Yb.L$^1$] and 5:1 for [Yb.L$^2$]. Several exchange pairs were observed in the EXSY spectra of [Yb.L$^1$], (ESI: Figure S10), whereas cross peaks were more difficult to observe with [Yb.L$^2$], emphasising the difference in their dynamic exchange behaviour. Using EXSYCalc for two EXSY spectra with 5 ms and 100 ms mixing times (looking at pyridine H$^4$), it was possible to estimate a $k_1$ rate for [Yb.L$^1$] of 54 s$^{-1}$ was estimated, 50 times faster than for [Y.L$^2$], and a $k_{-1}$ value of 16 s$^{-1}$. These rate values are consistent with rates of SAP to TSAP isomerisation observed in related 12N4 lanthanide complexes. [24]

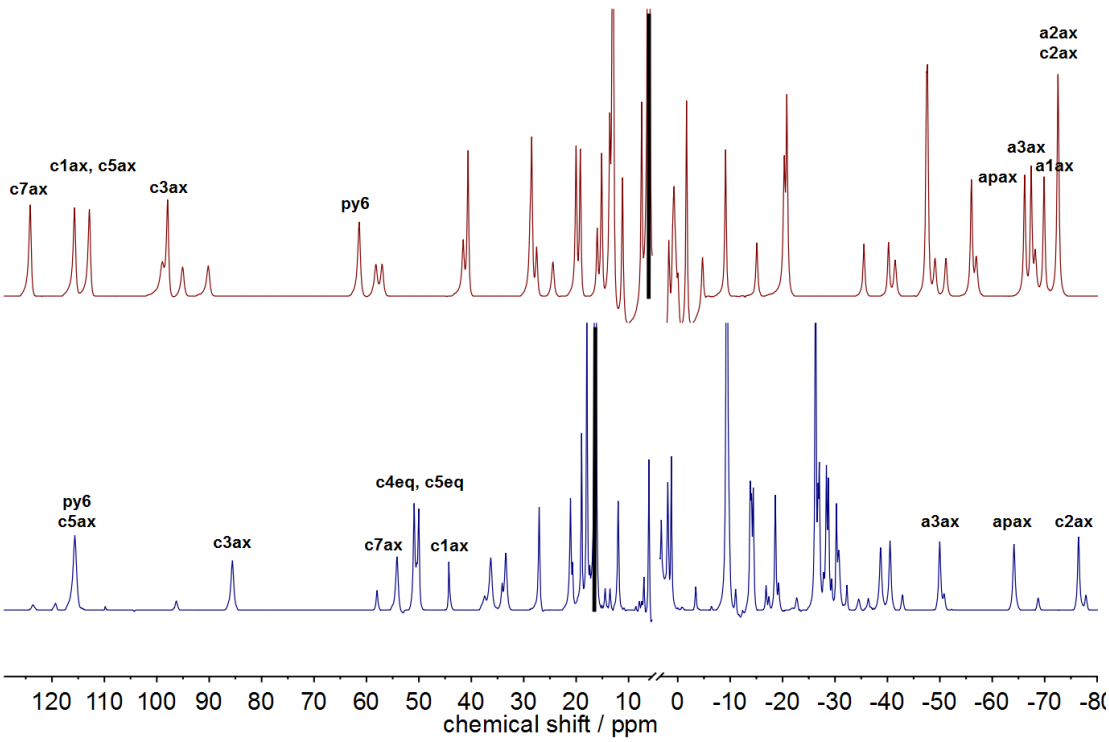


**Figure 4**. $^1$H NMR spectrum of [Yb.L$^1$] (*red*) and [Yb.L$^2$] (*blue*) (4.7 T, $D_2O$, 295 K); spectra have been vertically clipped to aid clarity; (full assignments are given in ESI Tables S3 and S6). The $^t$Bu signals are marked with vertical bars. The labels are given in Figure S5).

Simultaneous assignment and fitting of the proton and phosphorus paramagnetic shifts to the susceptibility tensor was carried out using the DFT optimized structures of (*RRR*)-*Λ*-(*λλλλ*) conformers (ESI: Table S8) and automated combinatorial fitting procedure developed and implemented in *Spinach 1.9*. Longitudinal relaxation rates and the linewidths have also been taken into account during the assignment process. The final assignments (Table S3, Figure S18) are in agreement with the observed COSY cross-peaks. Notably, the cyclen protons of the axial positions ('c1ax', 'c3ax', 'c5ax' and 'c7ax') form a well separated group in the case of [Yb.L$^1$], but they are more separated in the case of [Yb.L$^2$]; a similar effect is observed for axial protons in the exocyclic $CH_2$ groups.

The 'best-fit' traceless susceptibility tensors, (ESI: Tables S4 and S7: Figures S22 and S18), can be converted to axiality and rhombicity parameters and three Euler angles, with respect to the molecular frame. The z-axis of molecular frame points towards the centre of four nitrogen atoms of cyclen and the x-axis points towards the N1 atom (**Error! Reference source not found.**). Comparison of the CASSCF computed susceptibility anisotropy and the PCS fitted values are shown below (Table 6).

**Table 6.** Anisotropy of the susceptibility tensors of [Yb.L$^1$] and [Yb.L$^2$], extracted from paramagnetic shift fitting and computed with CASSCF. Axiality is shown in the Å$^3$ in SI units and Euler angles in zy'z" convention; the maximum value of rhombicity/axiality is defined as 1/3 (see computational details and ESI).

| | axiality, Å$^3$ | rhombicity/axiality | α ° | β ° | γ ° |
|---|---|---|---|---|---|
| [Yb.L$^1$] NMR | 0.127 | 0.163 | 58 | 4 | 54 |
| [Yb.L$^1$] CASSCF | 0.268 | 0.135 | 26 | 86 | 167 |
| [Yb.L$^2$] NMR | 0.113 | 0.140 | 185 | 23 | 300 |
| [Yb.L$^2$] CASSCF | 0.139 | 0.114 | 204 | 29 | 111 |

Computed axiality is larger than that extracted from PCS by about a factor of two for [Yb.L$^1$] and by 20% for [Yb.L$^2$]. In each case, it can be ascribed to systematic overestimation of the axiality, owing to the lack of dynamical correlation in CASSCF. The modulation of the ligand field by the surrounding water molecule is also not taken

into account. To tackle the latter effect, we have also computed susceptibility for each complex with one explicit water molecule; indeed, for [Yb.L$^1$] it led to a reduction of axiality by about 20% (Table S5). The reconstructed PCS fields based on the best-fit susceptibility tensors are presented at the Figure 5. Since the amplitude of the anisotropy is almost the same for both compounds the radial part of PCS field is very similar. The intermediate ratio of rhombicity/axiality manifests itself in the flattening of the otherwise axially symmetric blue region of the PCS field (Figure 5). The most important difference between [Yb.L$^1$] and [Yb.L$^2$] is the orientation of the PCS field that is mainly defined by $\beta$ angle of the susceptibility tensor (Table 6).

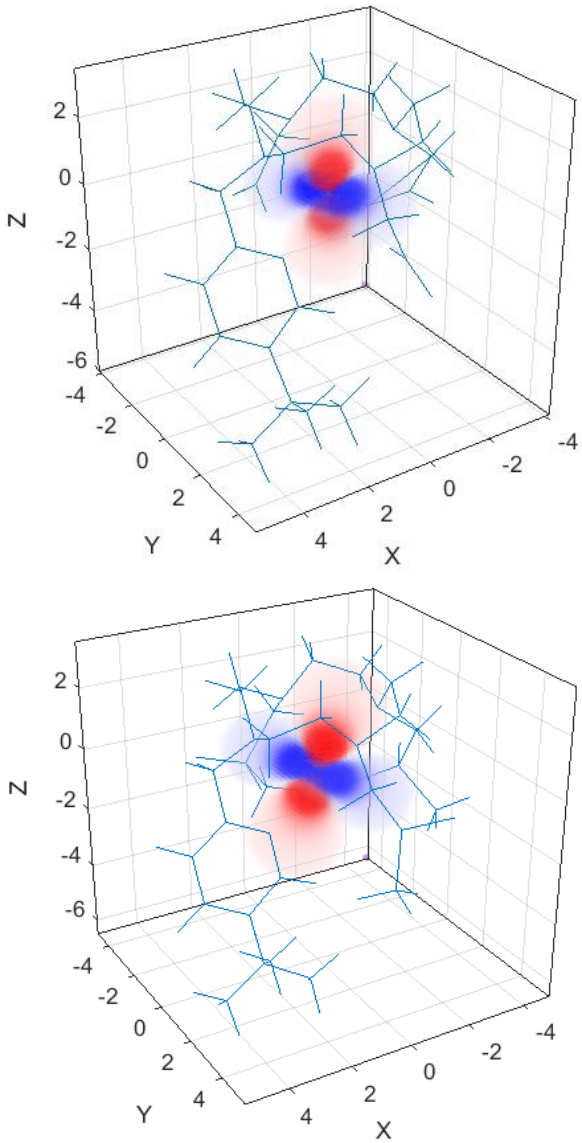


**Figure 5.** Pseudocontact shift (PCS) field reconstructed using the best fit susceptibility tensor for [Yb.L$^1$] (*top*) and [Yb.L$^2$] (*bottom*) created in *Spinach*.

The difference in the orientation of the PCS field is also responsible for the interchange in the order of the paramagnetic shifts observed in NMR (Figure 4).

## SUMMARY AND CONCLUSIONS

The lanthanide(III) complexes of $L^2$ are prototypical examples of PARASHIFT NMR contrast agents that are being developed for use in magnetic resonance spectral imaging *in vivo*. Understanding their structure and solution dynamics is an important part of appreciating why they behave so well for this role. [19-22]

The twisted square anti-prismatic lanthanide complexes of $L^2$ exist as two isomers differing in free energy in solution by only a few kJ/mol that undergo exchange by cooperative arm rotation. They give rise to pseudocontact shifts of the $^t$Bu reporter resonance that are 50 or 60 ppm greater compared to the tricarboxylate analogues based on $L^1$ for Dy, Tb and Tm complexes. In terms of the distance between the paramagnetic centre and the average position of the $^t$Bu hydrogen nuclei, the X-ray studies reveal that in [Yb.$L^1$] the distances range from 5.28 to 7.95Å ($10^3/\langle r^3\rangle$ = 3.76 Å$^{-3}$), whereas for [Yb.$L^2$], corresponding values are 5.46 to 8.05Å ($10^3/\langle r^3\rangle$ = 3.82 Å$^{-3}$). Evidently, the greater $^t$Bu shift found in [Ln.$L^2$] compared to [Ln$L^1$] is not due to a shorter distance. Detailed analysis of all PCS shifts shows that it is the difference in the orientation of the magnetic susceptibility tensor for the two complexes, rather than its anisotropy, that accounts very well for their markedly different NMR spectral behaviour. [19]

## EXPERIMENTAL SECTION

### X-ray crystallography

The X-ray single crystal data for [Yb.L$^1$]·2MeOH·$H_2O$ and [Yb.L$^2$]·EtOH·2$H_2O$ were collected using Mo-*K*α radiation (λ =0.71073Å) on a Bruker D8 Venture (Photon100 CMOS detector, IμS-microsource, focusing mirrors) diffractometer equipped with a Cryostream (Oxford Cryosystems) open-flow $N_2$ cryostat. Both structures were solved by direct method and refined by full-matrix least squares on $F^2$ for all data using Olex2 [35] and SHELXL [36] software. All non-hydrogen atoms were refined anisotropically, hydrogen atoms were placed in the calculated positions and refined in riding mode. [Yb.L$^1$] was a 2-component non-merohedral twin with component ratio 0.930:0.070(1), [Yb.L$^2$] as an inversion twin with component ratio 0.489:0.511(7).

*Crystal data*: $C_{24}H_{36}N_5O_6Yb$·2$CH_3OH$·$H_2O$, $M$ = 745.72, monoclinic, space group $P2_1/c$ (no. 14), $a$ = 13.4134(7), $b$ = 16.7937(9), $c$ = 14.9527(8) Å, β = 119.464(2)°, $V$ = 2932.6(3) Å$^3$, $Z$ = 4, $D_{calc}$ = 1.689 g cm$^{-3}$, μ = 3.25 mm$^{-1}$, $T$ = 120 K, 69043 reflections with θ ≤ 30.5° ($R_{merg}$ = 0.082), 381 refined parameters, final w$R_2(F^2)$ = 0.063 (on 7804 unique data), conventional $R_1(F)$ = 0.035 on 4783 data with $I \geq 2\sigma$, CCDC-1502162.

$C_{24}H_{45}N_5O_6P_3Yb$·$C_2H_6O$·2$H_2O$, $M$ = 847.70, monoclinic, space group $P2_1$ (no. 4), $a$ = 9.5975(4), $b$ = 13.8670(6), $c$ = 26.4618(11) Å, β = 99.837(2)°, $V$ = 3470.0(3) Å$^3$, $Z$ = 4, $D_{calc}$ = 1.623 g cm$^{-3}$, μ = 2.89 mm$^{-1}$, $T$ = 120 K, 94524 reflections with θ ≤ 34.9° ($R_{merg}$ = 0.032), 820 refined parameters, final w$R_2(F^2)$ = 0.060 (on 28857 unique data), conventional $R_1(F)$ = 0.032 on 25209 data with $I \geq 2\sigma$, CCDC-1501473.

### NMR and mass spectroscopy

$^1$H, $^{13}$C and $^{31}$P NMR spectra were recorded in commercially available deuterated solvents on a Bruker Avance-400 ($^1$H at 400.06 MHz, $^{13}$C at 100.61 MHz and $^{31}$P at 161.95 MHz), a Mercury 400 ($^1$H at 399.95 MHz), a Varian VNMRS-600 ($^1$H at 599.67 MHz, $^{13}$C at 150.79 MHz and $^{31}$P at 242.75 MHz), or a Varian VNMRS-700 ($^1$H at 699.73 MHz, $^{13}$C at 175.95 MHz and $^{31}$P at 283.26 MHz). All chemical shifts are given in ppm, with coupling constants are in Hz.

Electrospray mass spectra were obtained on a TQD mass spectrometer equipped with an Acquity UPLC system, an electrospray ion source and an Acquity photodiode array detector (Waters Ltd., UK). Accurate masses were recorded on an LCT Premier XE mass spectrometer or a QToF Premier Mass spectrometer, both equipped with an Acquity UPLC, a lock-mass electrospray ion source and an Acquity photodiode array detector (Waters Ltd., UK). Methanol was used as the carrier solvent.

## Electronic structure theory

Initial geometry optimization was done using BP86 [37] exchange-correlation functional followed by re-optimization and thermochemical analysis with M06-2X.[38] Solvent effects were included using the SMD model (water).[39] All calculations used cc-pVDZ [40] basis set with Stuttgart ECP [41] on the lanthanide. D3 dispersion correction was used to account for weak interactions.[42] The resolution of identity approximation with the corresponding auxiliary basis sets was used to speed up the calculations.[43] DFT calculations were carried out with the Gaussian09.[44]

Magnetic susceptibility tensors were computed in MOLCAS 8.0 [45] using CASSCF method [46] and relativistic ANO-RCC-VDZP basis set [47]. Spin-orbit coupling of 7 spin-free states of $4f^{13}$ configuration has been taken into account in RASSI module [48] followed by SINGLE_ANISO calculation of the magnetic susceptibility tensors.

Fitting of the paramagnetic shifts to the magnetic susceptibility tensors was carried out in *Spinach* 1.9 package [49]. Fermi contact terms were assumed to be negligible for all protons and phosphorous atoms. Point model for pseudocontact shift (PCS) has been used for all simulations [50]. Eigenvalues of the fitted susceptibility tensors were ordered to satisfy $|\chi_x|<|\chi_y|<|\chi_z|$, then axiality was computed as $3/2\chi_z$ and rhombicity as $(\chi_x-\chi_y)/2$. With this definition, the ratio between the rhombicity and the axiality falls between 0 and 1/3, the former yielding a $d_{z2}$ orbital like spatial profile and the latter yielding a $d_{yz}$ orbital like spatial profile. ZYZ convention was used for the Euler angles.

## Characterisation

The synthesis of the ligands $L^{1-3}$ and the method of preparation of their lanthanide(III) and yttrium complexes has been reported earlier. [19, 22]

**[Y.L$^1$]** (see ESI Table S3 for detail)

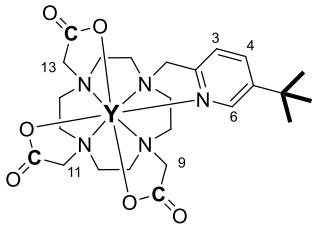

$^1$H NMR (600 MHz, $D_2O$, pD 6) δ (ppm) 8.47 (s, $H^{6py}$), 7.93 (d, $^3J_{HH}$ = 8.0 Hz, $H^{4py}$), 7.31 (d, $^3J_{HH}$ = 8.0 Hz, $H^{3py}$), 4.26 (d, $^2J_{HH}$ = -15.0 Hz, py$C\underline{H}_2$N), 3.84 (d, $^2J_{HH}$ = -15.0 Hz, py$C\underline{H}_2$N), 3.60-3.50 (m, N$C\underline{H}_2$NCOO-), 3.45-3.25 (m, cyclen-$C\underline{H}_2$), 3.22-3.11 (m, N$C\underline{H}_2$NCOO- ), 2.96 (d, $^2J_{HH}$ = -17.5 Hz, N$C\underline{H}_2C^9$OO-) 2.87-2.78 (m, cyclen-$C\underline{H}_2$), 2.76-2.51 (m, cyclen-$C\underline{H}_2$), 2.47-2.31 ((m, N$C\underline{H}_2C^9OO^-$/cyclen-$C\underline{H}_2$), 2.24-2.17 (m, cyclen-$C\underline{H}_2$), 1.63-1.55 (m, cyclen-$C\underline{H}_2$), 1.19 (s, $C(C\underline{H}_3)_3$). $^{13}$C NMR (150 MHz, $CDCl_3$,) δ (ppm) 146.4 ($C^{6py}$), 137.7 ($C^{4py}$), 121.9 ($C^{3py}$), 66.2 (py$\underline{C}H_2$N), 66.0 ($C^9$), 65.8 ($C^{11}$ and $C^{13}$), 56.8-54.8 (cyclen-$\underline{C}H_2$), 33.1 ($\underline{C}(CH_3)_3$). ESI-LRMS (+) *m/z* 580.2 [M+H]+; ESI-HRMS (+) *m/z* calcd. $C_{24}H_{37}N_5O_6Y$ 580.1802, found 580.1815.

**[Y.L$^2$]** (ESI Table S6, for detail)

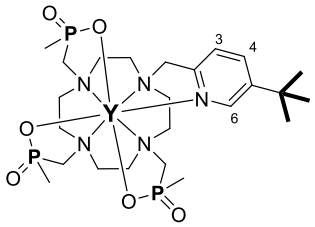

$^1$H NMR (600 MHz, $D_2O$) δ (ppm) 8.92 (s, $H^{6py}$ minor), 8.60 (s, $H^{6py}$ major), 7.97 (d, $^3J_{HH}$ = 8.0 Hz, $H^{4py}$ major), 7.91 (d, $^3J_{HH}$ = 8.0 Hz, $H^{4py}$ minor), 7.35 (d, $^3J_{HH}$ = 8.0 Hz, $H^{3py}$ major), 7.30 (d, $^3J_{HH}$ = 8.0 Hz, $H^{3py}$ minor), 4.55 (d, $^2J_{HH}$ = -16.0 Hz, py$C\underline{H}_2$N), 3.85-3.77 (m, cyclen-$C\underline{H}_2$), 3.64 (d, $^2J_{HH}$ = -16.0 Hz, py$C\underline{H}_2$N), 3.61.3.32 (m, N$C\underline{H}_2$P/cyclen-$C\underline{H}_2$), 3.01-2.94 (m, cyclen-$C\underline{H}_2$), 2.80-2.74 (m, N$C\underline{H}_2$P), 2.66-2.35 (m, N$C\underline{H}_2$P/cyclen-$C\underline{H}_2$), 2.34-2.26 (m, cyclen-$C\underline{H}_2$), 1.53 (d, $^2J_{PH}$ = 13.0 Hz, P$C\underline{H}_3$ minor), 1.46-1.42 (m, P$C\underline{H}_3$), 1.29-1.22 (m, P$C\underline{H}_3$/ $C(C\underline{H}_3)_3$), 1.24 ($C(C\underline{H}_3)_3$). $^{13}$C NMR (150 MHz, $CDCl_3$,) δ (ppm) 148.0 ($C^{6py}$ minor), 145.2 ($C^{6py}$ major), 138.4 ($C^{4py}$ major), 137.8 ($C^{4py}$ minor), 123.6 ($C^{3py}$ major), 123.0 ($C^{3py}$ minor), 59.3 (py$\underline{C}H_2$N), 55.5/56.3/56.0 (3×d, $^2J_{PC}$ = 95 Hz P$\underline{C}H_2$N major),

53.9/53.4/53.2/53.6/51.7/51.6/51.5/50.1 (cyclen-$\underline{C}H_2$ major), 18.7 (d, $^2J_{PC}$ = 95 Hz, P$\underline{C}H_3$ minor), 16.3/15.7/15.6 (3×d, $^2J_{PC}$ = 95 Hz, P$\underline{C}H_3$ major), 33.3 ($\underline{C}(CH_3)_3$), 29.9 ($C(\underline{C}H_3)_3$ major). $^{31}P\{^1H\}$ NMR (243 MHz, $D_2O$,) 44.0 ($^2J_{YP}$ = 5 Hz, $PCH_3$ minor), 43.9 ($^2J_{YP}$ = 5 Hz, $PCH_3$ major), 43.3 ($^2J_{YP}$ = 5 Hz, $PCH_3$ major), 43.0 ($^2J_{YP}$ = 5 Hz, $PCH_3$ minor), 41.0 ($^2J_{YP}$ = 6 Hz, $PCH_3$ major), 40.2 ($^2J_{YP}$ = 6 Hz, $PCH_3$ minor). ESI-LRMS (+) *m/z* 682.2 [M+H]+; ESI-HRMS (+) *m/z* calcd. for $C_{24}H_{45}N_5O_6P_3Y$ 682.1720, found 682.1714.

**[$H_2Y.L^3$]**

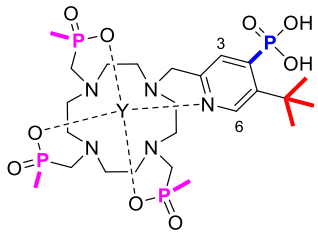

$^1H$ NMR (600 MHz, $D_2O$) δ (ppm) 8.96 (d, $^4J_{HP}$ =5.5 Hz, $H^{6py}$ minor), 8.64 (d, $^4J_{HP}$ =5.5 Hz, $H^{6py}$ major), 7.93 (d, $^3J_{HP}$ =13.5 Hz, $H^{3py}$ major), 7.88 (d, $^3J_{HP}$ =13.5 Hz, $H^{3py}$ minor), 4.55 (d, $^2J_{HH}$ = -15.5 Hz, py$\underline{C}H_2$N major), 3.80 (m, cyclen-$\underline{C}H_2$), 3.66 (d, $^2J_{HH}$ = -15.5 Hz, py$\underline{C}H_2$N major), 3.63-3.33 (m, cyclen-$\underline{C}H_2$/N$\underline{C}H_2$P), 3.22-3.14 (m, cyclen-$\underline{C}H_2$), 3.04-2.94 (m, cyclen-$\underline{C}H_2$), 2.82-2.75 (m, N$\underline{C}H_2$P), 2.66-2.24 (m, N$\underline{C}H_2$P/cyclen-$\underline{C}H_2$), 2.34-2.26 (m, cyclen-$\underline{C}H_2$), 1.53 (d, $^2J_{PH}$ = 14.0 Hz, P$\underline{C}H_3$ minor), 1.45 (d, $^2J_{PH}$ = 14.0 Hz, P$\underline{C}H_3$ major), 1.28 (d, $^2J_{PH}$ = 14.0 Hz, P$\underline{C}H_3$ major), 1.26 (d, $^2J_{PH}$ = 14.0 Hz, P$\underline{C}H_3$, major), 1.23 (d, $^2J_{PH}$ = 14.0 Hz, P$\underline{C}H_3$ minor), 1.19 (d, $^2J_{PH}$ = 14.0 Hz, P$\underline{C}H_3$ minor), 1.46 (s, $C(\underline{C}H_3)_3$). $^{13}C$ NMR (150 MHz, $CDCl_3$,) δ (ppm) 146.7 ($C^{6py}$ major), 129.0 ($C^{3py}$ major), 59.6 (py$\underline{C}H_2$N major), 55.6/56.3/56.0 (3×d, $^2J_{PC}$ = 95 Hz P$\underline{C}H_2$N major), 53.9/53.5/53.2/52.6/51.8/51.7/51.6/50.1 (cyclen-$\underline{C}H_2$ major), 35.3 ($\underline{C}(CH_3)_3$), 30.7 ($C(\underline{C}H_3)_3$ major), 13.0/16.4/15.7 (3×d, $^2J_{PC}$ = 95 Hz, P$\underline{C}H_3$ major). $^{31}P\{^1H\}$ NMR (243 MHz, $D_2O$,) 44.1 ($^2J_{YP}$=5 Hz, $PCH_3$ minor), 44.0 ($^2J_{YP}$=5 Hz, $PCH_3$ major), 43.4 ($^2J_{YP}$=5 Hz, $PCH_3$ major), 43.0 ($^2J_{YP}$=5 Hz, $PCH_3$ minor), 41.0 ($^2J_{YP}$=5 Hz, $PCH_3$ major), 39.7 ($^2J_{YP}$=5 Hz, $PCH_3$ minor), 7.9 (P(O)OOH minor), 7.5 (P(O)OOH minor); ESI-LRMS (+) *m/z* 762.6 [M+H]+; ESI-HRMS (+) *m/z* calcd. for $C_{24}H_{46}N_5O_9P_4Y$ 762.1383, found 762.1388.

## ASSOCIATED CONTENT

**Supporting Information**.

The Supporting Information is available free of charge on the ACS Publications website at DOI: 10.1021/acs.inorg- chem.xxxxxx

Crystallographic data (CIF) The data have been deposited at the Cambridge Crystallographic Data Centre as supplementary publication CCDC-1502162 and CCDC-1501473.

## AUTHOR INFORMATION

**Corresponding Author** *E-mail: david.parker@dur.ac.uk

**Notes**

The authors declare no competing financial interest.

## ACKNOWLEDGMENTS and DEDICATION

We thank the ERC (FCC 266804) and EPSRC (EP/N006909/1; EP/L01212X/1; EP/N006895/1) for support. The authors also acknowledge the use of the IRIDIS High Performance Computing Facility, and associated support services at the University of Southampton, in the completion of this work. This paper is dedicated to the memory of Professor Leone Spiccia (Monash).

## REFERENCES

(1) Macrocyclic metal complexes for metalloenzyme mimicry and sensor development**,** Joshi, T.; Graham, B.; Spiccia, L. *Acc. Chem. Res*. **2015**, *48*, 2366-2379.

(2) The ubiquitous DOTA and its derivatives: the impact of 1,4,7,10-tetraazacyclododecane-1,4,7,10-tetraacetic acid on biomedical imaging, Stasiuk, G. J.; Long, N. J. *Chem. Commun*. **2013**, *49*, 2732-2746.

(3) (a) MR imaging probes: design and applications, Boros, E.; Gale, E. M.; Caravan, P. *Dalton Trans*. **2015**, *44*, 4804-4818; (b) Lanthanide Probes for Bioresponsive Imaging, Heffern, M. C.; Matosiuk, L. M.; Meade, T. J. *Chem. Rev*. **2014**,*114*, 4496.

(4) (a) Matching chelators to radiometals for radiopharmaceuticals, Price, E. W.; Orvig, C. *Chem. Soc. Rev*. **2014**, *43*, 260-290; (b) A nuclear chocolate box: the periodic table of nuclear medicine, Blower, P. J. *Dalton Trans*. **2015**, *44*, 4819-4844.

(5) Six-coordinate Iron (II) and Cobalt (II) paraSHIFT Agents for Measuring Temperature by Magnetic Resonance Spectroscopy, Tsitovich, P. B.; Cox, J. M.; Benedict, J. B.; Morrow, J. R. *Inorg. Chem.* **2016,** *55*, 700-716.

(6) Paramagnetic fluorine labelled lanthanide complexes as probes for 19-F magnetic resonance imaging and spectroscopy, Chalmers, K. H.; De Luca, E.; Hogg, N. M. H.; Kenwright, A. M.; Kuprov, I.; Parker, D.; Botta, M.; Wilson, J. I.; Blamire, A. M. *Chem.-Eur. J*. **2010**, *16*, 134-148.

(7) Lanthanide complexes as paramagnetic probes for 19-F magnetic resonance, Harvey, P.; Kuprov, I.; Parker, D. *Eur. J. Inorg. Chem.* **2012**, 2015-2022.

(8) Moving the goal posts: enhancing the sensitivity of PARASHIFT proton magnetic resonance imaging and spectroscopy, Harvey, P. Blamire, A. M.; Wilson, J. I.; Finney, K-L. N. A.; Funk, A. M.; Senanayake, P. K.; Parker, D. *Chem. Sci.* **2013**, *4*, 4251-4256.

(9) Boosting $^{19}$F MRI - SNR-efficient detection of paramagnetic contrast agents using ultra-fast sequences, Schmid, F.; Holtke, C.; Parker, D.; Faber, C. *Magn. Reson. Med*. **2013**, *69*, 1056-1062.

(10) Contrast agents possessing high temperature sensitivity, Milne, M.; Hudson, R. H. E. *Chem. Commun*. **2011**, *47*, 9194-9196.

(11) Lanthanides as shift and relaxation agents in elucidating the structure of proteins and nucleic acids, Geraldes, C. F. G. C.; Luchinat, C. *Met. Ions. Biol. Syst*. **2003**, *40*, 513.

(12) Characterisation and evaluation of paramagnetic fluorine labelled glycol chitosan conjugates for $^{19}$F and $^{1}$H magnetic resonance imaging, De Luca, E.; Harvey, P.; Chalmers, K. H.; Mishra, A.; Senanayake, P. K.; Wilson, J. I.; Botta, M.; Fekete, M.; Blamire, A. M.; Parker, D. *J. Biol. Inorg. Chem.* **2014**, *19*, 215-227.

(13) Responsive fluorinated lanthanide probes for magnetic resonance spectroscopy, Senanayake, P. K.; Kenwright, A. M.; Parker, D.; van der Hoorn, S. K. *Chem. Commun.*, **2007**, 2923–2925.

(14) 19-F NMR based pH probes: lanthanide(III) complexes with pH sensitive chemical shifts , Kenwright, A. M.; Kuprov, I.; De Luca, E.; Parker, D.; Pandya, S. U.; Senanayake, P. K.; Smith, D. G. *Chem. Commun*. **2008**, *22*, 2514-2516.

(15) (a) Brain temperature by Biosensor Imaging of Redundant Deviation in Shifts (BIRDS): comparison between $TmDOTP^{5-}$ and $TmDOTMA^{-}$, Coman, D.; Trubel, H. K.; Hyder, F. *NMR Biomed.*, **2010**, *23*, 277-285; (b) In vivo three-dimensional molecular imaging with Biosensor Imaging of Redundant Deviation in Shifts (BIRDS) at high spatiotemporal resolution, Coman, D.; de Graaf, R. A.; Rothman, D. L.; Hyder, F. *NMR Biomed*. **2013**, *26*, 1589-1593.

(16) Paramagnetic 19-F chemical shift probes probes that respond selectively to calcium or citrate levels and signal ester hydrolysis , Harvey, P.; Mishra, A.; Chalmers, K. H.; De Luca, E.; Parker, D. *Chem.-Eur. J.* **2012**, *18*, 8748-8757.

(17) (a) Strategies to enhance signal intensity with paramagnetic fluorine-labelled lanthanide complexes as probes for 19-F magnetic resonance , Chalmers, K. H.; Botta, M.; Parker, D. *Dalton Trans.* **2011**, *40*, 904-913; (b) Aime, S.; Botta, M. Ermondi, G. *Inorg. Chem*. **1992**, *31*, 4291; (c) Tsitovich, P. B.; Morrow, J. R. *Inorg. Chim,. Acta*, **2012**, *393*, 3.

(18) (a) NMR studies of neutral lanthanide complexes with tetraazamacrocyclic ligands containing three phosphinate and one carboxamide coordinating arms, Aime, S.; Botta, M.; Parker, D.; Williams, J. A. G. *Dalton Trans*. **1995**, 2259-2266; (b) The degree of hydration of octadentate macrocyclic ligands incorporating phosphinate donors : solution relaxometry and luminescence studies, Aime, S.; Botta, M.; Parker, D.; Williams, J. A. G.; *J. Chem. Soc., Dalton Trans*. **1996**, 17-23; (c) Non-radiative deactivation of the excited states of europium, terbium and ytterbium complexes by energy matched OH, NH and CH oscillators: an improved luminescence method for establishing solution hydration states, Beeby, A.; Clarkson, I. M.; Dickins, R. S.; Faulkner, S.; Parker, D.; Royle, L.; de Sousa, A. S.; Williams, J. A. G.; Woods, M.; *J. Chem. Soc., Perkin Trans. 2*, **1999**, 493-503.

(19) (a) Critical analysis of the limitations of Bleaney's theory of magnetic anisotropy in lanthanide coordination complexes, Funk, A. M.; Finney, K-L. N. A.; Harvey, P.; Kenwright, A. M.; Neil, E. R.; Rogers, N. J.; Senanayake, P. K.; D. Parker, *Chem. Sci.* **2015**, *6*, 1655-1662; (b) Electromagnetic susceptibility anisotropy and its importance for paramagnetic NMR and optical spectroscopy in lanthanide coordination chemistry, Blackburn, O. A.; Edkins, R. M.; Faulkner, S.; Kenwright, A. M.; Parker, D.; Rogers, N. J.; Shuvaev, S. *Dalton Trans*. **2016**, *45*, 6782-6800.

(20) (a) Another challenge to paramagnetic relaxation theory: a study of paramagnetic proton NMR relaxation in closely related series of pyridine-derivatised dysprosium complexes, Rogers, N. J.; Finney, K-L. N. A.; Senanayake, P. K.; Parker, D. *Phys. Chem. Chem. Phys*. **2016**, *18*, 4370-4376; (b) Challenging lanthanide relaxation theory: erbium and thulium complexes that show NMR relaxation rates faster than dysprosium and terbium analogues Funk, A. M.; Harvey, P.; Finney, K-L. N. A.; Fox, M. A.; Kenwright, A. M.; Rogers, N. J.; Senanayake, P. K.; Parker, D. *Phys. Chem. Chem. Phys*. **2015**, *17*, 16507-16511.

(21) A new paramagnetically shifted imaging probe for MRI, Senanayake, P. K.; Rogers, N. R. ; Harvey, P.; Finney, K-L. N. A. ; Funk, A. M. ; Parker, D. ; Wilson, J. I. ; Maxwell, R.; Blamire, A. M. *Magn. Reson. Med*. **2016**, in press, DOI 10.1002/mrm.26185.

(22) Simultaneous triple imaging with two PARASHIFT probes: encoding anatomical, pH and temperature information using magnetic resonance shift imaging, Finney, K-L. N. A.; Harnden, A.C.; Rogers, N. C.; Senanayake, P. K. ; Blamire, A. M. ; O'Hogain, D.; Parker, D, *Chem. Sci*., **2016**, *7*, submitted.

(23) Structural studies of lanthanide complexes of macrocyclic ligands bearing benzylphosphinate groups, Aime, S.; Batsanov, A. S.; Botta, M.; Dickins, R. S.; Faulkner, S.; Foster, C. E.; Harrison, A.; Howard, J. A. K.; Moloney, J. M.; Norman, T. J.; Parker, D.; Royle, L.; Williams, J. A. G. *J. Chem. Soc., Dalton Trans*. **1997,** 3623-3636.

(24) Being excited by lanthanide coordination chemistry: aqua species, chirality, excited state chemistry and exchange dynamics, Parker, D.; Dickins, R. S.; Puschmann, H.; Crossland, C.; Howard, J. A. K. *Chem Rev*. **2002**, *102*, 1977.

(25) (a) Synthesis and characterisation of dimeric eight-coordinate lanthanide(III) complexes of a macrocyclic tribenzylphosphinate ligand, Senanayake, K.; Thompson, A. L.; Howard, J. A. K.; Botta, M.; Parker, D. *Dalton Trans*. **2006**, 5423; (b) One example of useful disorder : Structure of Pr(III) complex of 1,4,7,10-tetraazacyclododecane-10-methyl-1,4,7-tris(methylenephenylphosphinic) acid, Klimentova, J.; Vojtisek, P.; *J. Mol. Struct*.

**2007**, *826*, 82; (c) Derivative of cyclen with three methylene(phenyl)phosphinic acid pendant arms. Synthesis and crystal structures of its lanthanide complexes, Rohovec, J.; Vojtisek, P.; Hermann, P.; Lukes, I.; *J. Chem. Soc. Dalton, Trans*. **2000**, 141; (d) Lanthanide(III) complexes of aminoethyl-DO3A as PARACEST contrast agents based on decoordination of the weakly bound amino group, Krchova, T.; Kotek, J.; Janak, D.; Havlickova, J.; Cisarova, I.; Hermann, P.; *Dalton Trans.* **2013**, 42, 15735-15747; (e) Crystal Structures of Lanthanide(III) Complexes with Cyclen Derivative Bearing Three Acetate and One Methylphosphonate Pendants, Vojtíšek, P.; Cígler, P.; Kotek, J.; Rudovský, J.; Hermann, P.; Lukeš, I.; *Inorg. Chem.* **2005**, 44, 5591-5599; (f) Lanthanide(III) Complexes of Pyridine-*N*-Oxide Analogues of DOTA in Solution and in the Solid State. A New Kind of Isomerism in Complexes of DOTA-like Ligands, Polášek, M.; Kotek, J.; Hermann, P.; Císařová, I.; Binnemans, K.; Lukeš, I.; *Inorg. Chem.* **2009**, 48, 466-475.

(26) (a) New lanthanide complexes for sensitized visible and near-IR light emission: synthesis, 1H NMR, and X-ray structural investigation and photophysical properties, Quici, S.; Marzanni, G.; Forni, A.; Accorsi, G.; Barigelletti, *Inorg. Chem.* **2004**, *43*, 1294; (b) Structure and relaxivity of macrocyclic gadolinium complexes incorporating pyridyl and 4-morpholinopyridyl substituents, Aime, S.; Batsanov, A. S.; Botta, M.; Howard, J. A. K.; Lowe, M. P.; Parker, D. *New J. Chem.* **1999**, *23*, 669; (c) 1,2,4-Triazine method of bipyridine ligand synthesis for the preparation of new luminescent Eu(III) complexes, Prokhorov, A. M.; Kozhevnikov, V. N.; Kopchuk, D. S.; Bernard, H.; Le Bris, N.; Tripier, R.; Handel, H.; Koenig, B. *Tetrahedron* **2011**, *67*, 597.

(27) (a) A list of organic kryptoracemates, Fabian, L.; Brock, C. P. *Acta Crystallogr*. **2010**, *B66*, 94-103; (b) A list of organometallic krypto- racemates, Bernal, I.; Watkins, S. *Acta Crystallogr*. **2015**, *C71*, 216-221.

(28) *P*1 or *P*1$^{\bar{}}$? Or something else?, Marsh, R.E. *Acta Crystallogr*. **1999**, *B55*, 931-936.

(29) Absolute configurations of Emycin D, E and F; mimicry of centrosymmetric space groups by mixtures of chiral stereoisomers, Walker, M.; Pohl, E.; Herbst-Irmer, R.; Gerlitz, M.; Rohr, J.; Sheldrick, G.M. *Acta Crystallogr*. **1999**, *B55*, 607-616.

(30) Density functionals with broad applicability in chemistry, Zhao, V.; Truhlar, D. G. *Acc. Chem. Res*. **2008**, *41*, 157-167.

(31) Pure shift NMR, Zangger, K. *Progress in Nuclear Magnetic Resonance Spectroscopy*, 2015, **86-87**, 1–20

(32) Pure Shift $^{1}$H NMR: A Resolution of the Resolution Problem?, Aguilar, J. A.; Faulkner, S.; Nilsson, M.; Morris, G. A. *Angew. Chem. Int. Ed.* **2010**, *122*, 3901-3903.

(33) Minimising Research Bottlenecks by Decluttering NMR Spectra, Aguilar, J. A.; Cassani, J.; Delbianco, M.; Adams, R. W.; Nilsson, M.; Morris, G. A.; *Chem. Eur. J.*, **2015**, *21*, 6623-6630.

(34) Ultrahigh-resolution NMR spectroscopy, Foroozandeh, M.; Adams, R. W.; Meharry, N. J.; Jeannerat, D.; Nilsson, M.; Morris, G. A. *Angew. Chem. Int. Ed.*, **2014**, *53*, 6990–6992.

(35) Olex2: A complete structure solution, refinement and analysis program, Dolomanov, O. V.; Bourhis, L. J.; Gildea, R. J.; Howard J. A. K.; Puschmann, H. *J. Appl. Crystallogr.*, **2009**, *42*, 339-341.

(36) (a) A short history of SHELX, Sheldrick, G. M. *Acta Crystallogr.* **2008**, *A64*, 112-122; (b) Crystal structure refinement with SHELXL, Sheldrick, G. M. *Acta Crystallogr.* **2015**, *C71*, 3-8.

(37) (a) Density-functional exchange-energy approximation with correct asymptotic behavior, Becke, A. D. *Phys Rev A* **1988**, *38*, 3098; (b) Density-functional approximation for the correlation energy of the inhomogeneous electron gas, Perdew, J. P. *Phys Rev B* **1986**, *33*, 8822.

(38) The M06 suite of density functionals for main group thermochemistry, thermochemical kinetics, noncovalent interactions, excited states, and transition elements: two new functionals and systematic testing of four M06-class functionals and 12 other functionals, Zhao, Y.; Truhlar, D. G. *Theor. Chem. Acc*., **2008**, *120*, 215.

(39) Universal solvation model based on solute electron density and on a continuum model of the solvent defined by the bulk dielectric constant and atomic surface tensions, Marenich, A. V.; Cramer, C. J.; Truhlar, C. G. *J. Phys. Chem. B* **2009**, *113*, 6378.

(40) Gaussian basis sets for use in correlated molecular calculations. I. The atoms boron through neon and hydrogen, Dunning Jr. T. H. , *J. Chem. Phys*., **1989**, *90*, 1007-23.

(41) Energy-adjusted ab initio pseudopotentials for the first row transition elements, Dolg, M.; Wedig, U.; Stoll, H.; Preuss, H. *J. Chem. Phys*. **1987**, *86*, 866.

(42) A consistent and accurate ab initio parametrization of density functional dispersion correction (DFT-D) for the 94 elements H-Pu**,** Grimme, S.; Antony, J.; Ehrlich, S.; Krieg, H. *J. Chem. Phys*., **2010**, *132* 154104.

(43) Robust and variational fitting: Removing the four-center integrals from center stage in quantum chemistry, Dunlap, B. I. *J. Mol. Struct. (Theochem)*, **2000**, *529*, 37-40.

(44) Gaussian 09, Revision D.01, M.J. Frisch, G.W. Trucks, H.B. Schlegel, G.E. Scuseria, M.A. Robb, J. R. Cheeseman, G. Scalmani, V. Barone, B. Mennucci, G.A. Petersson, H. Nakatsuji, M. Caricato, X. Li, H.P. Hratchian, A.F. Izmaylov, J. Bloino, G. Zheng, J.L. Sonnenberg, M. Hada, M. Ehara, K. Toyota, R. Fukuda, J. Hasegawa, M. Ishida, T. Nakajima, Y. Honda, O. Kitao, H. Nakai, T. Vreven, J.A. Montgomery,Jr., J.E. Peralta, F. Ogliaro, M. Bearpark, J.J. Heyd, E. Brothers, K.N. Kudin, V.N. Staroverov, R. Kobayashi, J. Normand, K. Raghavachari, A. Rendell, J.C. Burant, S.S. Iyengar, J. Tomasi, M. Cossi, N. Rega, J.M. Millam, M. Klene, J.E. Knox, J.B. Cross, V. Bakken, C. Adamo, J. Jaramillo, R. Gomperts, R.E. Stratmann, O. Yazyev, A.J. Austin, R. Cammi, C. Pomelli, J.W. Ochterski, R.L. Martin, K. Morokuma, V.G. Zakrzewski, G. A. Voth, P. Salvador, J.J. Dannenberg, S. Dapprich, A.D. Daniels, Ö. Farkas, J.B. Foresman, J.V. Ortiz, J. Cioslowski, D.J. Fox, Gaussian, Inc., Wallingford CT, 2009.

(45) Aquilante, F.; Autschbach, J.; Carlson, R. K.; Chibotaru, L. F.; Delcey, M. G.; De Vico, L.; Fdez. Galván, I.; Ferré, N.; Frutos, L. M.; Gagliardi, L.; Garavelli, M.; Giussani, A.; Hoyer, C. E.; Li Manni, G.; Lischka, H.; Ma, D.; Malmqvist, P. Å.; Müller, T.; Nenov, A.; Olivucci, M.; Pedersen, T. B.; Peng, D.; Plasser, F.; Pritchard, B.; Reiher, M.; Rivalta, I.; Schapiro, I.; Segarra-Martí, J.; Stenrup, M.; Truhlar, D. G.; Ungur, L.; Valentini, A.; Vancoillie, S.; Veryazov, V.; Vysotskiy, V. P.; Weingart, O.; Zapata, F.; Lindh, R. Molcas 8: New capabilities for multiconfigurational quantum chemical calculations across the periodic table. *J. Comput. Chem.* **2016**, 37 (5), 506-541.

(46) Roos, B. O.; Taylor, P. R.; Siegbahn, P. E. M. A Complete Active Space Scf Method (CASSCF) Using a Density-Matrix Formulated Super-CI Approach. Chem Phys **1980**, 48 (2), 157-173.

(47) (a) Roos, B. O.; Lindh, R.; Malmqvist, P.-Å.; Veryazov, V.; Widmark, P.-O.; Borin, A. C. New Relativistic Atomic Natural Orbital Basis Sets for Lanthanide Atoms with Applications to the Ce Diatom and LuF3. *The Journal of Physical Chemistry A* **2008**, 112 (45), 11431-11435. (b) Roos, B. O.; Lindh, R.; Malmqvist, P.-Å.; Veryazov, V.; Widmark, P.-O. Main Group Atoms and Dimers Studied with a New Relativistic ANO Basis Set. *The Journal of Physical Chemistry A* **2004**, 108 (15), 2851-2858.

(48) Malmqvist, P. Å.; Roos, B. O.; Schimmelpfennig, B. The restricted active space (RAS) state interaction approach with spin–orbit coupling. *Chem. Phys. Lett.* **2002**, 357 (3–4), 230-240.

(49) Hogben, H. J.; Krzystyniak, M.; Charnock, G. T. P.; Hore, P. J.; Kuprov, I. Spinach – A software library for simulation of spin dynamics in large spin systems. *J. Magn. Reson.* **2011**, 208 (2), 179-194.

(50) Suturina, E. A.; Kuprov, I. Pseudocontact shifts from mobile spin labels. *Phys. Chem. Chem. Phys.* **2016**, 18 (38), 26412-26422.

**For Table of Contents Only**

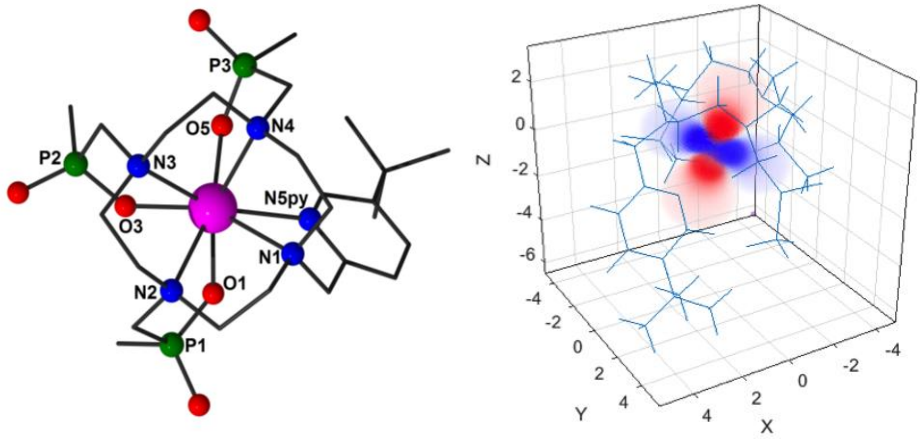


Eight-coordinate ytterbium complexes with a bound pyridine group adopt a twisted square antiprismatic coordination geometry; the orientation of the pseudocontact shift field is mainly defined by the $\beta$ angle of the magnetic susceptibility tensor.